ACS Catalysis

Research Article

pubs.acs.org/acscatalysis

A Single Glycosidase Harnesses Different Pyranoside Ring Transition State Conformations for Hydrolysis of Mannosides and Glucosides

Anupong Tankrathok,[†,‡] Javier Iglesias-Fernández,[§] Rohan J. Williams,[∥] Salila Pengthaisong,[†] Supaporn Baiya,[†] Zalihe Hakki,[∥] Robert C. Robinson,[⊥,#] Maria Hrmova,[○] Carme Rovira,[*,§,△] Spencer J. Williams,[*,∥] and James R. Ketudat Cairns[*,†,□]

[†]School of Biochemistry, Institute of Science, and Center for Biomolecular Structure, Function and Application, Suranaree University of Technology, Nakhon Ratchasima 30000, Thailand

[‡]Department of Biotechnology, Faculty of Agro-Industrial Technology, Rajamangala University of Technology, Isan, Kalasin Campus, Kalasin 46000, Thailand

[§]Departament de Química Orgànica/Institut de Química Teòrica i Computacional (IQTCUB), Universitat de Barcelona, Martí i Franquès 1, 08028 Barcelona, Spain

[∥]School of Chemistry and Bio21 Molecular Science and Biotechnology Institute, University of Melbourne, Parkville, Victoria 3010, Australia

[⊥]Institute of Molecular and Cell Biology, A*STAR (Agency for Science, Technology and Research), Biopolis, Singapore 138673

[#]Department of Biochemistry, National University of Singapore, 8 Medical Drive, Singapore 117597

[○]School of Agriculture, Food and Wine, Australian Centre for Plant Functional Genomics, University of Adelaide, Waite Campus, Glenn Osmond, Australia

[△]Institució Catalana de Recerca i Estudis Avançats (ICREA), Passeig Lluís Companys, 23, 08018 Barcelona, Spain

[□]Laboratory of Biochemistry, Chulabhorn Research Institute, Bangkok 10210, Thailand

Supporting Information

ABSTRACT: Hydrolysis of β-D-mannosides by β-mannosidases typically proceeds via a $B_{2,5}$ transition state conformation for the pyranoside ring, while that of β-D-glucosides by β-glucosidases proceeds through a distinct $^4H_3$ transition state conformation. However, rice Os7BGlu26 β-glycosidase hydrolyzes 4-nitrophenyl β-D-glucoside and β-D-mannoside with similar efficiencies. The origin of this dual substrate specificity was investigated by kinetic, structural, and computational approaches. The glycosidase inhibitors glucoimidazole and mannoimidazole inhibited Os7BGlu26 with K_i values of 2.7 nM and 10.4 μM, respectively. In X-ray crystal structures of complexes with Os7BGlu26, glucoimidazole bound to the active site in a ^4E conformation, while mannoimidazole bound in a $B_{2,5}$ conformation, suggesting different transition state conformations. Moreover, calculation of quantum mechanics/molecular mechanics (QM/MM) free energy landscapes showed that 4-nitrophenyl β-D-glucoside adopts a $^1S_3/^4E$ conformation in the Michaelis complex, while 4-nitrophenyl β-D-mannoside adopts a $^1S_5/B_{2,5}$ conformation. The QM/MM simulations of Os7BGlu26 catalysis of hydrolysis also supported the itineraries of $^1S_3 \rightarrow {}^4E/{}^4H_3{}^{‡} \rightarrow {}^4C_1$ for β-D-glucosides and $^1S_5 \rightarrow B_{2,5}{}^{‡} \rightarrow {}^OS_2$ for β-D-mannosides, thereby revealing that a single glycoside hydrolase can hydrolyze glycosides of different configurations via distinct transition state pyranoside conformations.

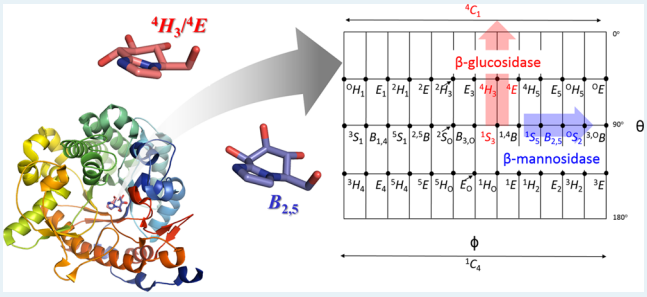

KEYWORDS: *β-glucosidase, β-mannosidase, QM/MM metadynamics, structural analysis, transition state mimic, X-ray crystallography*

INTRODUCTION

β-Glucosidases and β-mannosidases are enzymes of significant biological and biotechnological importance. β-Glucosidases assist in the catabolism of glycolipids and plant cell wall polysaccharides, as well as release of defense compounds, phytohormone activation, and alkaloid biosynthesis.[1] β-Mannosidases play important roles in N-linked glycoprotein catabolism in eukaryotes,[2] in flowering and seed germination in plants,[3,4] and in biomass utilization by bacteria.[5] Both types of enzymes are of interest in second-generation biofuel production from plant cell-wall-derived materials.[6]

A conformational itinerary for an enzyme describes the changes in molecular shape of a substrate molecule as it progresses along

Received: July 21, 2015
Revised: August 26, 2015
Published: August 28, 2015

DOI: 10.1021/acscatal.5b01547
ACS Catal. 2015, 5, 6041−6051

the reaction coordinate. For glycoside hydrolases (GHs), the identification of conformational itineraries is a subject of ongoing interest, providing insights into the stereoelectronic strategies used for enzymatic catalysis and potentially guiding the design of enzyme inhibitors.[7] The conformational itineraries of β-D-mannoside and β-D-glucoside hydrolysis by β-mannosidases (E.C. 3.2.1.25) and β-glucosidases (E.C. 3.2.1.21), respectively, have been analyzed in detail and typically proceed through different transition states.[8−11]

On the basis of their protein sequences, β-mannosidases have been classified into glycoside hydrolase (GH) families GH1, GH2, and GH5 within the carbohydrate active enzyme (CAZy) classification system (www.cazy.org).[12] All three families contain enzymes that act with retention of anomeric stereochemistry and are classified into clan GH-A, the members of which have a classic triose phosphate isomerase (TIM) $(\beta/\alpha)_8$ barrel structure with two catalytic glutamic acid residues.[12] X-ray crystal structures have been reported for β-mannosidases representing all three families (e.g., see refs 11, 13, and 14). While most plant GH1 β-glucosidases exhibit little β-mannosidase activity, rice (*Oryza sativa*) GH1 β-glycosidase Os7BGlu26[14] is of particular interest, as it belongs to a group of GH1 enzymes that have dual β-glucosidase and β-mannosidase activities, including rice BGlu1 (designated here as Os3BGlu7),[15] barley HvBII,[16,17] and *Arabidopsis thaliana* BGLU44.[18] Rice Os7BGlu26 represents an extreme case, as it hydrolyzes 4-nitrophenyl (4NP) β-D-mannosides and β-D-glucosides with similar efficiency (k_{cat}/K_M is 3-fold higher for 4NP β-D-mannoside (4NPMan) than for 4NP β-D-glucoside (4NPGlc)).[14,17] The structural, electronic, and mechanistic bases of this substrate promiscuity are not well understood.

Kinetic isotope effect studies with substrates for which either glycosylation or deglycosylation is rate limiting have demonstrated that retaining glycosidase catalysis occurs through "exploded" transition states (TS) with oxocarbenium ion like character (Figure 1a).[19] In these TS, a partial double bond between C1 and the endocyclic oxygen stabilizes the charge that develops on C1 as the glycosidic bond is broken by electron delocalization across the C1−O5 bond. The partial double bond character between the anomeric carbon and the endocyclic oxygen engenders a trigonal-planar geometry about these centers, demanding that the atoms C5−O5−C1−C2 are coplanar, or nearly so, at the TS. Ring conformations that comply with this requirement include the two boat ($B_{2,5}$ and $^{2,5}B$) and two half-chair ($^4H_3$ and $^3H_4$) conformations and the closely related ^4E, E_4, ^3E, and E_3 envelope conformations. Figure 1b shows a Mercator representation of all conformations of a pyranose ring, upon which the transition-state compliant conformations are identified.[9,20−24]

Retaining β-glucosidases are thought to pass through a $^1S_3 \rightarrow {}^4H_3^{\ddagger} \rightarrow {}^4C_1$ itinerary in the glycosylation step (Figure 1a, bottom).[8] For example, the structure of a Michaelis complex of cellulase Cel5A from *Bacillus agaradhaerens* with a β-cellobioside substrate analogue revealed a $^1S_3$ conformation, and that of the glycosyl enzyme intermediate displayed a relaxed $^4C_1$ conformation.[8] This evidence suggests that a $^4H_3$ or closely related ^4E conformation is attained at the transition state on the basis of the principle of least nuclear motion.[25,26] In support of this, a transition state mimicking complex with a cellobiose-derived imidazole revealed binding in a ^4E conformation.[27] Evidence for the same itinerary has been found for a number of β-glucosidases,[28−34] including Os3BGlu7.[35]

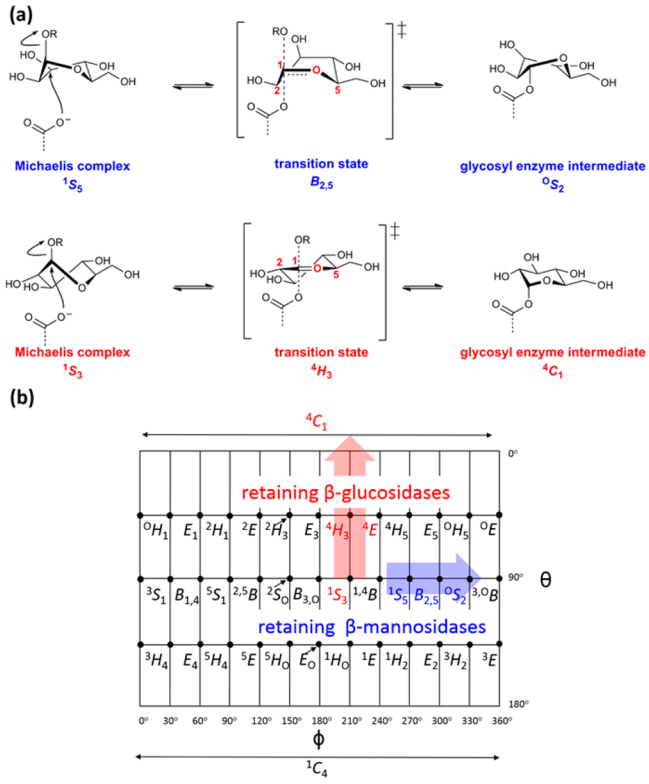

Figure 1. Mechanism and conformational itinerary of glycoside hydrolysis by retaining β-mannosidases and β-glucosidases. (a) Glycosylation step of the retaining mechanism for hydrolysis of β-D-mannosides by β-mannosidases (top) and hydrolysis of β-D-glucosides by β-glucosidases (bottom). The second (deglycosylation) step is the reverse of this process. The atoms of the pyranose rings that must be coplanar to allow partial double-bond formation in the oxocarbenium ion transition state are emphasized in red. (b) Mercator plot of possible pyranose conformations with the conformational pathways observed in the glycosylation step of β-mannosidases ($^1S_5 \rightarrow B_{2,5}^{\ddagger} \rightarrow {}^OS_5$) and β-glucosidases ($^1S_3 \rightarrow {}^4H_3^{\ddagger} \rightarrow {}^4C_1$) highlighted by blue and red arrows, respectively.

In contrast to β-glucoside hydrolysis, structural studies of Michaelis complexes,[9,36] glycosyl enzyme species,[9] and TS mimicking inhibitors[11,24] have provided support for a $^1S_5 \rightarrow B_{2,5}^{\ddagger} \rightarrow {}^OS_2$ itinerary for enzymatic β-mannoside/β-mannan hydrolysis (Figure 1a, top). For example, in an analysis of 25 prospective β-mannosidase TS analogues with the family GH2 *Bt*Man2A, Tailford et al.[11] described the aryl mannoimidazoles as the "most persuasive transition state mimics" due to their near linear free energy relationship and observed $B_{2,5}$ conformations in complexes with the enzyme.[13,37,38] The ability of mannoimidazole to mimic the TS has also been assessed by quantum mechanics. A recent study showed that the mechanistically relevant boat ($^{2,5}B$ or $B_{2,5}$), half-chair ($^4H_3$ and $^3H_4$), and envelope (^3E, E_3, ^4E, and E_4) conformations of mannoimidazole are energetically accessible in its conformational free energy landscape (FEL).[39] This fact, which does not generally apply for more conformationally biased inhibitors such as isofagomine,[39] suggests that glycoimidazoles may in general be informative of TS conformations of GHs.

Although the TS of β-D-mannoside hydrolysis by GH2, GH26, and GH113 β-mannosidases/β-mannanases have been analyzed in detail, the TS conformation(s) of enzymes that have dual β-mannosidase and β-glucosidase activities remain unclear. Using a combination of kinetic analysis and X-ray crystallographic studies

DOI: 10.1021/acscatal.5b01547
ACS Catal. 2015, 5, 6041−6051

of transition state mimicking inhibitors, and quantum mechanics evaluation of substrate conformational flexibility and reaction trajectories, we provide compelling evidence that the plant GH1 β-glycosidase Os7BGlu26 achieves efficient catalysis of two different sugar configurations by hydrolyzing β-D-glucosides via a $^{1}S_{3} \rightarrow {}^{4}E/{}^{4}H_{3}^{\ddagger} \rightarrow {}^{4}C_{1}$ itinerary and β-D-mannosides through a $^{1}S_{5} \rightarrow B_{2,5}^{\ddagger} \rightarrow {}^{O}S_{2}$ itinerary.

EXPERIMENTAL SECTION

Protein Expression, Purification, and Crystallization. Recombinant Os3BGlu7, Os7BGlu26, and HvBII proteins were expressed and purified as previously described.[14,17,40] The Os7BGlu26 protein was concentrated and crystallized by the hanging drop vapor diffusion method with microseeding, as previously described.[14] Conditions for crystallization were optimized from the previously reported 0.8 M K,Na tartrate, 0.1 M Na HEPES, pH 7.25 conditions by varying the salt, buffer, and protein concentration. Prior to data collection, the crystals were soaked in precipitant containing 20% (v/v) glycerol with 50 mM mannoimidazole, 50 mM glucoimidazole, or 50 mM isofagomine. The crystals were flash vitrified and kept at liquid nitrogen temperature.

Data Collection and Processing and Structure Refinement. The X-ray diffraction data for Os7BGlu26 structures in complexes with the inhibitors were collected at the BL13B1 beamline at the National Synchrotron Radiation Research Center (NSRRC), Hsinchu, Taiwan, with a 1.0 Å wavelength X-ray beam and an ADSC Quantum 315 CCD detector. All data sets were indexed, integrated, and scaled with the HKL-2000 package.[41]

The Os7BGlu26 complex structure was solved by rigid body refinement of the native Os7BGlu26 structure (PDB code 4JHO) followed by refinement with REFMAC5[42] in the CCP4 suite of programs.[43] Model building was performed with the COOT program.[44] The quality of the final models was assessed with PROCHECK[45] and MolProbity.[46] Graphic representations of structures were generated in PyMol (Schrödinger LLC). The sugar ring forms were assessed via visual inspection and by calculation of the Cremer−Pople ring puckering parameters[47] on the Cremer−Pople calculator Web site (http://www.ric.hi-ho.ne.jp/asfushi/).

Kinetic Constants with Mannosides and Glucosides. The products of hydrolysis of β-1,4-mannobiose and methyl β-D-mannoside were determined from duplicate reactions by high-performance anion exchange chromatography (HPAEC) with a mannose standard curve, as previously described for glucose.[48] For methyl β-D-glucoside, the glucose released in triplicate reactions was measured with the Sigma-Aldrich glucose oxidase/peroxidase kit according to the supplier's instructions. All three enzymes have maximum activity in the pH 4−5 range, with >90% maximal activity at pH 5.0.[17] Reactions were conducted in 50 mM sodium acetate buffer, pH 5.0, containing 1 μg/μL of BSA at 30 °C for times that gave a linear rate of release and the initial rates, V_0, in preliminary time course studies. Depending on the rates, substrate concentration/solubility, and apparent K_M values, the k_{cat}/K_M values were determined by nonlinear regression of Michaelis−Menten plots when the substrate concentrations covered the range of 0.3−3 times the K_M value (in the case of methyl β-D-glucoside for all enzymes), by linear regression of Michaelis−Menten plots at substrate concentrations at least 8-fold lower than the K_M value (Os7BGlu26 and HvBII with mannobiose and Os3BGlu7 with methyl β-D-mannoside), or by linear reciprocal (Lineweaver−Burk) plots when the substrate concentration range was near the K_M value but not bracketing it sufficiently for accurate nonlinear regression (Os3BGlu7 with mannobiose and Os7BGlu26 and HvBII with methyl β-D-mannoside).

Determination of Inhibition Constants. Mannoimidazole, glucoimidazole, and isofagomine were evaluated as inhibitors. Initial time courses indicated that the inhibition was maximum after 90−120 min. For Os7BGlu26, K_i values were determined by incubating 0.5 μg of enzyme in 50 mM sodium acetate buffer, pH 5.0, containing 1 μg/μL BSA, and inhibitor at 30 °C for 120 min. The residual enzyme activities were monitored by assaying activity toward 0.2, 0.5, and 0.75 mM 4NPMan at 30 °C for 25 min. For Os3BGlu7, 0.2 μg of enzyme was used, and the residual enzyme activity was monitored by assaying activity toward 0.1, 0.2, and 0.5 mM 4NPGlc at 30 °C for 15 min. For HvBII, 0.5 μg of enzyme was used, and the residual enzyme activity was monitored by assaying activity toward 0.1, 0.2, 0.3, 0.5, and 0.75 mM 4NPMan at 30 °C for 45 min. The residual activity of each enzyme was measured as 4NP released per minute, monitored at 405 nm, after alkalinization of the assay solution with sodium carbonate. For K_i value determinations, five to seven inhibitor concentrations bracketing the K_i value were assayed (for HvBII, higher concentrations at which uncompetitive inhibition became significant were eliminated from the analysis). K_i values were calculated by solution of the linear regression equations of Dixon plots of inhibitor concentrations versus $1/V$ values[49] and by a proportionally robust fit[50] of the data in GraFit 5.0.

Slow onset inhibition was assessed with 4NPMan as the substrate for Os7BGlu26. The enzyme was incubated with inhibitors (5 μM mannoimidazole, 0.01 μM glucoimidazole, or 0.1 μM isofagomine) for 10 min or 2 h in 50 mM sodium acetate, pH 6.5, containing 1 μg/μL BSA at 25 °C. After this time, 4NPMan was added to the enzyme/inhibitor solution to 1 mM final concentration. The released 4NP was monitored at 405 nm every 30 s thereafter.

Classical Molecular Dynamics Simulations. Classical molecular dynamics (MD) simulations were performed to equilibrate the Michaelis complex structures of Os7BGlu26 with 4NPGlc and 4NPMan. The initial structures of the complexes were obtained by docking of the substrates in the active site, as previously described.[14] The protonation states and hydrogen atom positions of all histidine residues were selected on the basis of their hydrogen bond network. All Asp and Glu residues were taken as deprotonated (i.e., negatively charged) except Glu179 (the catalytic acid−base residue, which is known to be protonated at the pH optimum of glycosidases due to the proximity of the negatively charged nucleophile residue).[51] One sodium ion was added to achieve neutrality of the protein structure. The system was initially subjected to classical MD using Amber11 software.[52] The protein was modeled with the FF99SB force field,[53] and the GLYCAM06 parameter set[54] was used for the carbohydrate molecules. The 4NP aglycon was parametrized in the antechamber module of Amber11, with atomic charges derived from an ESP charge calculation using the Gaussian03 software package.[55] The LEAP module of the AMBER program was used to solvate the system, which is composed of 7652 protein atoms and approximately 15000 water molecules, enclosed in a box of 80 × 82 × 75 Å. All water molecules were described with the TIP3P force field.[56] The MD simulations were performed with a time step of 1 fs and periodic boundary conditions with full electrostatics computed by the particle mesh Ewald method.[57] Nonbonded interactions were computed at

DOI: 10.1021/acscatal.5b01547
ACS Catal. 2015, 5, 6041−6051

every step using the default cutoff distance of 8 Å. The systems were equilibrated in several steps. First, all solvent molecules were relaxed with a gradient minimizer, holding the protein and substrate fixed. Next, the whole system was allowed to relax. To gradually reach the desired temperature of 300 K, spatial constraints were initially added to the protein and substrate, while the water molecules and sodium ion were allowed to move freely. The constraints were then removed and the whole system was allowed to reach the desired temperature of 300 K, using the Berendsen weak coupling method.[58] The simulation was continued for 100 ps at constant pressure, allowing the cell volume to evolve. The Berendsen weak coupling method was also used to maintain the pressure at 1 atm with isotropic position scaling. The MD simulations for the 4NPMan and 4NPGlc complexes were extended to 6 and 10 ns, respectively, until the systems had reached equilibrium. Analysis of the trajectories was carried out by using the standard tools of AMBER and VMD.[59] One snapshot from the end of each simulation was taken as the starting structure for the subsequent enzyme−substrate QM/MM simulations.

QM/MM Molecular Dynamics Simulations. QM/MM MD simulations were performed with the method developed by Laio et al.,[60] which combines Car−Parrinello molecular dynamics,[61] based on density functional theory (DFT), with force-field MD (for consistency, the same force fields as in the classical simulations were used). The QM region was taken as the 4NPGlc or 4NPMan molecule (36 atoms) for the calculations of sugar puckering. To simulate the glycosylation reaction, the catalytic nucleophile and acid/base residues were also included in the QM region (51 atoms). The QM systems were enclosed in an isolated orthorhombic box of size 14.8 Å × 18.0 Å × 15.9 Å (puckering simulation) and 18.5 Å × 18.0 Å × 18.0 Å (glycosylation reaction). The Kohn−Sham orbitals were expanded in a plane wave (PW) basis set with a kinetic energy cutoff of 70 Ry, and calculations employed ab initio pseudopotentials generated within the Troullier−Martins scheme.[62] The calculations were performed using the Perdew, Burke, and Ernzerhoff generalized gradient-corrected approximation (PBE),[63] which has been used in several studies of sugar conformational FELs.[38,64−67] A recent study on the potential energy profile of the glycosylation step of a GH shows that PBE results are similar to MP2 values (within 1−2 kcal/mol, depending on the basis set employed), with the mechanism being unaltered.[68] It is also worth noting that the conformational FEL of cyclohexane, computed with PBE and metadynamics, was found to be in very good agreement with experiments.[69] The fictitious mass for the electronic degrees of freedom of the CP Lagrangian was set at 500 au and the simulation time step at 0.12 fs. Both complexes were equilibrated at 300 K for around 10 ps before starting the metadynamics simulations of sugar puckering.

Metadynamics Simulations of Sugar Puckering and Glycosylation Reactions. QM/MM metadynamics simulations were performed to explore the conformational FEL of the β-glucosyl and β-mannosyl moieties in the two enzyme−substrate complexes. The Cremer−Pople[47] puckering coordinates θ and ϕ were used as collective variables, as described previously.[70] In metadynamics, the dynamics of the system was biased by the sequential addition of repulsive Gaussian-like potentials, which prevents it from revisiting previously sampled configurations and hence forces the system to escape from one minimum to another. We used the metadynamics driver provided by the Plumed2 plugin[71] combined with well-tempered metadynamics.[70] Initially, the height and the width of these Gaussian terms were set at 1 kcal mol^{-1} and 0.1 rad, respectively, for both systems. A temperature window of ΔT = 9300 K was used for the well-tempered approach,[70] with a deposition time of 48 fs. The simulations were stopped after having added 7051 Gaussians (4NPGlc complex) and 7717 Gaussians (4NPMan complex). The conformational FEL of isolated glucoimidazole was computed with the following setup (the corresponding parameters were selected from an analysis of the evolution of the system during the unbiased MD simulation and from the expected energy barrier heights): Gaussian height/width 0.2 kcal mol^{-1}/0.1 arbitrary unit, deposition time 60 fs; 11500 deposited Gaussians; ΔT = 3100 K.

Additional QM/MM metadynamics simulations were performed to model the glycosylation reactions for 4NPGlc and 4NPMan. One collective variable was considered, namely that corresponding to the difference of coordination numbers of the main bonds being broken/formed during the reaction (C1−O_{E389} and the C1−O_{4NP}). The coordination numbers were calculated from the following equation: $CN_{ij} = (1 - (d_{ij}/d_0)^p)/(1 - (d_{ij}/d_0)^{p+q})$, where the parameters were set as p = 6, q = 6, and d_0 = 2.3 Å. This is considered an appropriate approximation, since 4NP is a good leaving group such that the formation of the glycosyl enzyme intermediate needs little assistance from the acid/base residue. Moreover, it is unlikely that the conformational itinerary of the sugar ring is affected by the degree of protonation of the 4NP aglycon. The QM/MM metadynamics simulations were stopped after having added 1277 Gaussians (4NPGlc complex) and 2104 Gaussians (4NPMan complex). The following setup was used: Gaussian height/width 0.5 kcal mol^{-1}/0.015 arbitrary unit, deposition time 30 fs.

RESULTS AND DISCUSSION

Hydrolytic Preferences with Slow Mannoside and Glucoside Substrates. The relative substrate preferences of Os3BGlu7, Os7BGlu26, and HvBII have been previously defined by comparison of k_{cat}/K_M values for 4NP-glycosides bearing relatively good (i.e., low pK_a value) leaving groups (Table 1). To assess the preferences with "slower substrates" with poorer leaving groups that require general acid catalysis, we determined k_{cat}/K_M values for β-1,4-mannobiose and cellobiose. When studied using 4NPMan, HvBII is the most proficient β-mannosidase in terms of k_{cat}/K_M and possesses the highest preference for 4NPMan (13-fold higher k_{cat}/K_M value for 4NPMan versus 4NPGlc; Table 1). However, with slower substrates, while HvBII remained the most proficient in terms of k_{cat}/K_M, Os7BGlu26 had the greatest preference for mannobiose versus cellobiose (12-fold higher k_{cat}/K_M for mannobiose than cellobiose; Table 1). To probe whether the change in preference for a slower substrate reflected preferences for the aglycon structure or its lower nucleofugacity, methyl β-D-glucoside and methyl β-D-mannoside were also assessed; these substrates were more effective substrates for all three enzymes, with higher k_{cat}/K_M values, and the ratios of k_{cat}/K_M for mannoside- versus glucoside-configured substrates were in the same relative order as for mannobiose versus cellobiose for the three enzymes, but with higher mannoside preferences. In summary, using 4NP-substrates HvBII has the highest proficiency for β-D-mannosides and the greatest preference for mannosides. Conversely, using slow substrates, HvBII and Os7BGlu26 show similar proficiencies for mannosides and Os7BGlu26 displays the greatest preference for mannosides. Os3BGlu7 shows a strong preference for glucosides with either slow or fast substrates.

Kinetic Investigation of Inhibitor Binding. To understand the conformational pathway of β-D-mannoside and

DOI: 10.1021/acscatal.5b01547
ACS Catal. 2015, 5, 6041−6051

Table 1. Apparent Kinetic Parameters for Hydrolysis of β-D-Glucosides and β-D-Mannosides

substrate	parameter	Os7BGlu26	Os3BGlu7	HvBII
4NPMan	k_{cat}/K_M (mM^{-1} s^{-1})	2.11 ± 0.20[a]	1.01 ± 0.02[b]	12.7 ± 0.2[a]
4NPGlc	k_{cat}/K_M (mM^{-1} s^{-1})	0.63 ± 0.003[a]	35 ± 1[b]	1.00 ± 0.05[a]
	k_{cat}/K_M ratio	3.3	0.029	12.7
β-1,4-mannobiose	k_{cat}/K_M (mM^{-1} s^{-1})	0.323 ± 0.002	0.0029 ± 0.0002	1.68 ± 0.02
cellobiose	k_{cat}/K_M (mM^{-1} s^{-1})	0.026 ± 0.001[a]	0.050 ± 0.002[b]	5.8 ± 0.2[a]
	k_{cat}/K_M ratio	12	0.058	0.29
methyl β-D-Man	k_{cat}/K_M (μM^{-1} s^{-1})	7.3 ± 0.4	0.96 ± 0.004	8.1 ± 0.4
methyl β-D-Glc	k_{cat}/K_M (μM^{-1} s^{-1})	0.15 ± 0.002	4.8 ± 0.1	1.36 ± 0.05
	k_{cat}/K_M ratio	47	0.20	5.7

[a]Data from ref 17. [b]Data from ref 15.

Table 2. Data for Inhibition of GH1 Os7BGlu26, Os3BGlu7, and HvBII

	Os7BGlu26		Os3BGlu7		HvBII	
	K_i (M)	ΔG^a (kcal/mol)	K_i (M)	ΔG^a (kcal/mol)	K_i (M)	ΔG^a (kcal/mol)
glucoimidazole[b]	$(2.7 \pm 0.15) \times 10^{-9}$	−11.9	$(0.43 \pm 0.018) \times 10^{-9}$	−13.0	$(1.5 \pm 0.2) \times 10^{-9}$	−12.2
isofagomine[b]	$(135 \pm 6) \times 10^{-9}$	−9.5	$(118 \pm 5) \times 10^{-9}$	−9.6	$(17.2 \pm 1.6) \times 10^{-6}$	−10.8
mannoimidazole[b]	$(10.4 \pm 0.06) \times 10^{-6}$	−6.9	$(1.9 \pm 0.09) \times 10^{-6}$	−7.9	$(5.70 \pm 0.99) \times 10^{-6}$	−7.3

[a]$\Delta G = RT \ln K_i$[80] where the temperature was 303 K. [b]Chemical structures for the inhibitors are shown in Chart S1 in the Supporting Information.

β-D-glucoside hydrolysis in plant GH1 enzymes with dual specificity, we first assessed a series of putative transition state mimics, based on their shape, charge, and in some cases planarity, as well as their potency.[23,72] Inhibitors were assessed for binding to Os7BGlu26 and HvBII β-mannosidases and Os3BGlu7 β-glucosidase by kinetic inhibition studies. Inhibition was observed with the K_i values in the following order: glucoimidazole > isofagomine > mannoimidazole (Table 2). No inhibition was observed for glucotetrazole, 1-deoxynojirimycin, or 1-deoxymannojirimycin at 100 μM (data not shown). It is of note that Os7BGlu26, HvBII, and Os3BGlu7 display a strikingly higher affinity for glucoimidazole in comparison to mannoimidazole: 3850-, 3800-, and 4420-fold, respectively, corresponding to a 5 kcal mol^{-1} difference in binding energy in each case, despite the preferences of Os7BGlu26 and HvBII for mannosides, in terms of k_{cat}/K_M values as described above.

Slow onset inhibition is sometimes observed for transition state mimics and, in cases where it occurs, is believed to arise from the slow accumulation of the more tightly bound TS conformation of the inhibitor in the active site, although we highlight slow onset inhibition is not necessary or sufficient for a TS analogue.[72] All three inhibitors exhibit slow onset inhibition of Os7BGlu26, as shown by a greater inhibition of 4NPMan hydrolysis by Os7BGlu26 after 2 h preincubation than after 10 min preincubation (Figure S1 in the Supporting Information). Although Os7BGlu26 has a pH optimum range of 4.0−5.0 and apparent pK_a value of the catalytic acid base of 5.0−5.5,[17] these experiments were performed at pH 6.5 to allow a continuous assay; thus, part of the slow onset may be due to slow kinetics for formation of appropriately charged pairs of inhibitor and enzyme. However, similar experiments done at pH 5.0 with stopped assays showed that maximum inhibition was achieved after approximately 90 min preincubation (data not shown), suggesting a similar slow onset inhibition mechanism at the optimal pH, despite the catalytic acid/base and imidazoles (glucoimidazole $pK_a = 6.12$)[73] being predominantly protonated at pH 5.0 and predominantly deprotonated at pH 6.5. Since the inhibitors are positively charged when protonated and the catalytic acid/base neutral when protonated (i.e., at pH 5.0), while the acid/base will be negatively charged when the inhibitor is largely neutral (at pH 6.5), the differences appear to be largely compensatory. These similar results at pH 5.0 and 6.5 suggest that the crystal structures, which were obtained at pH 7.25, may serve as reasonable models for the enzyme/inhibitor interactions at the optimum pH, despite differences in protonation that likely exist.

Structural Investigation of Inhibitor Binding to Os7BGlu26. Os7BGlu26 protein crystals soaked with mannoimidazole, glucoimidazole, or isofagomine provided X-ray diffraction data sets with resolutions of 2.00 Å (PDB code 4RE2), 2.55 Å (PDB code 4RE3), and 2.30 Å (PDB code 4RE4), respectively (Table S1 in the Supporting Information). In each complex, the inhibitor bound in the −1 subsite, but the three inhibitors adopted distinct conformations (Figure 2).

The Os7BGlu26 complex with mannoimidazole showed a distorted ring adopting a $B_{2,5}$ conformation (Figure 2a). This conformation is similar to the $B_{2,5}$ conformation seen for mannoimidazole bound to *B. thetaiotaomicron* GH2 β-mannosidase *Bt*Man2A[11] and is consistent with a $B_{2,5}$ conformation for the TS of β-D-mannoside hydrolysis. This structure, together with the previous Os7BGlu26 structure in a complex with D-mannose in a $^1S_5$ conformation,[14] is suggestive of a $^1S_5 \rightarrow B_{2,5}^{\ddagger} \rightarrow {}^OS_5$ conformational itinerary for the first step of mannoside hydrolysis mediated by GH1 enzymes, similar to that of GH2 β-mannosidases.

In contrast, the Os7BGlu26 complex with glucoimidazole revealed a ^4E conformation (Figure 2b), which is consistent with the $^4E/^4H_3$ TS proposed for hydrolysis of β-D-glucosides. The ^4E conformation was also observed in X-ray structures of glucoimidazole complexes with a GH1 myrosinase[31] and a GH1 β-glycosidase from *Thermotoga maritima* (*Tm*GH1)[33] and is suggestive of a $^1S_3 \rightarrow {}^4E/^4H_3^{\ddagger} \rightarrow {}^4C_1$ conformational itinerary for β-D-glucoside hydrolysis by Os7BGlu26. It is noteworthy that the pseudoequatorial position of the 2-hydroxyl in the $^4E/^4H_3$ conformation of glucoimidazole places O2 in nearly the same position as the corresponding atom in the $B_{2,5}$ conformation of mannoimidazole (Figures 2 and 3). This positional near equivalence of O2 is reminiscent of the comparison that has been made between the crystal structures of a β-D-glucoside in a $^4H_3$

DOI: 10.1021/acscatal.5b01547
ACS Catal. 2015, 5, 6041−6051

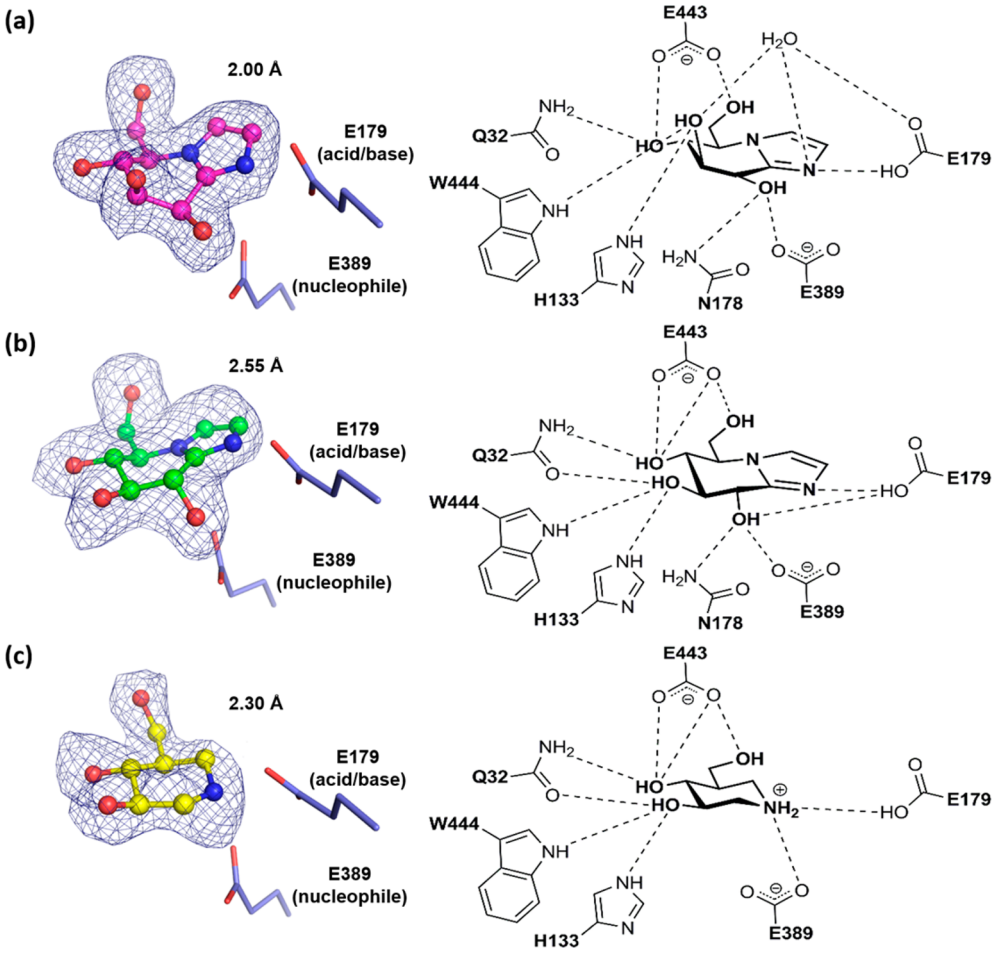

Figure 2. Structures of rice Os7BGlu26 in complex with (a) mannoimidazole, (b) glucoimidazole, and (c) isofagomine. The unbiased weighted $F_o - F_c$ (OMIT) electron density maps of the putative transition state mimic inhibitors are represented as a blue mesh contoured at 4σ (left panels), and the resolution of each data set is given. The hydrogen-bonding networks between the protein and the inhibitors are shown in the right panels.

conformation bound to the family GH1 *Tm*GH1 β-glucosidase and of a β-D-mannoside in a $B_{2,5}$ conformation bound to the family GH5 *Cm*Man5 β-mannosidase, which was proposed as an explanation as to why isofagomine lactam inhibits both β-glucosidases and β-mannosidases.[74] However, this is the first time this positional equivalence has been shown to occur within the active site of a single glycosidase, thereby explaining how the same enzyme has the ability to hydrolyze substrates of D-*gluco*- and D-*manno*-configured saccharides. Taken together, the conformations observed of the mannoimidazole and glucoimidazole bound to Os7BGlu26 strongly suggest that Os7BGlu26 hydrolyzes β-D-mannosides and β-D-glucosides via different TS conformations.

In the Os7BGlu26 complex with isofagomine, the piperidine ring is in a $^4C_1$ conformation, which is its lowest energy conformation.[39] This shape is also the relaxed conformation of D-glucosides and D-mannosides and corresponds to the conformation of this inhibitor in its complex with a GH1 β-glucosidase from *Thermotoga maritima*,[32] as well as to that of β-D-mannosyl-1,4-isofagomine in GH26 and GH113 β-mannanases.[39] Thus, despite the fact that the K_i value of isofagomine is 4.4-fold lower than that for mannoimidazole, the structure of the isofagomine complex does not display any of the distortion that would be expected for a transition state mimic.

The hydrogen-bond interactions among Os7BGlu26 and mannoimidazole, glucoimidazole, and isofagomine are shown in Figure 2. Mannoimidazole and glucoimidazole form hydrogen bonds with Q32, H133, N178, E179, E389, E443, and W444, although with key differences. Both carboxyl oxygens of E443 are within bonding distance of O4 of glucoimidazole, whereas only one oxygen is within this distance in the mannoimidazole complex. In contrast, Q32 only interacts with O4 of mannoimidazole but with both O3 and O4 of glucoimidazole. It is remarkable that by distortion of mannoimidazole to a $B_{2,5}$ conformation, and glucoimidazole to a ^4E conformation, the two epimeric inhibitors can achieve essentially the same interactions between the Os7BGlu26 active site residues and O2. However, as highlighted in Figure 3, the short (2.6 Å) hydrogen bond from Q32 to O3 seen in the glucoimidazole complex is absent in the mannoimidazole complex, owing to the greatly different positions of the inhibitor O3 in the two complexes. Isofagomine forms hydrogen bonds that are essentially equivalent to glucoimidazole at O3, but lacks O2; thus, it cannot form the hydrogen bonds to N178, E178, and E389 that occur with the imidazole inhibitors. Although isofagomine forms fewer hydrogen-bonding interactions, it is a more potent inhibitor than mannoimidazole. The relatively weak binding of mannoimidazole may reflect the energetic cost of distorting the piperidine ring to a $B_{2,5}$ conformation (calculated at 6 kcal mol^{-1})[39] and/or the displacements of active-site amino acid residues that allow mannoimidazole to make the same interactions as made by glucoimidazole in the ^4E conformation. Conversely, the stronger

DOI: 10.1021/acscatal.5b01547
ACS Catal. 2015, 5, 6041−6051

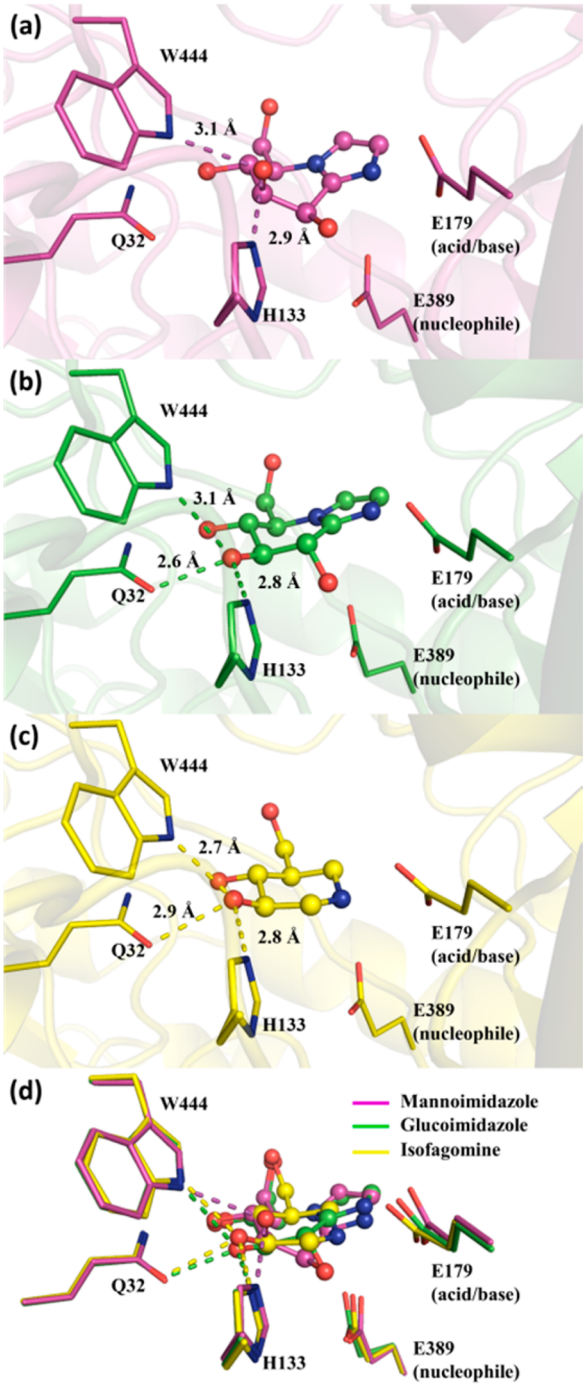

Figure 3. X-ray structures highlighting hydrogen bonds of rice Os7BGlu26 to O3 of (a) mannoimidazole, (b) glucoimidazole, and (c) isofagomine. The three structures are superimposed in (d) to show that while O2 is localized in an equivalent position in mannoimidazole and glucoimidazole (absent in isofagomine), O3 has divergent positions. For mannoimidazole, O3 makes fewer direct hydrogen bonds to the Os7BGlu26 protein. The putative hydrogen bonds were drawn between potential hydrogen bond donors and acceptors within 3.2 Å at positions where the angle among a potential hydrogen, the acceptor atom (A), and its bonded atom (B), H−A−B, is greater than 90° or is within 3.6 Å of ideal geometry.

binding of isofagomine in comparison to mannoimidazole may result from a stronger Coulombic interaction between the anionic nucleophile residue and the strongly basic (and presumably protonated) nitrogen of isofagomine, versus a possibly weaker Coulombic interaction between the acid/base and the less basic (but still presumably protonated) "anomeric" nitrogen of mannoimidazole.

Superposition of the active site structures of Os3BGlu7 and Os7BGlu26 provides insight into the β-glucosidase/β-mannosidase preferences of each enzyme (Figure S2 in the Supporting Information). The position of H133 is optimal to interact with the O3 of the $B_{2,5}$ conformation of mannoimidazole in Os7BGlu26 β-mannosidase, while H130 is in a position to interact with the a β-D-glucosyl residue or glucoimidazole in a $^4E/^4H_3$ conformation in Os3BGlu7. Similar subtle differences can be seen for the other residues interacting at the O3 and C2 position that may help to explain the enzymatic preferences.

Conformational Free Energy Landscape and Catalytic Itinerary of β-D-Mannoside and β-D-Glucoside Substrates Bound to Os7BGlu26. QM/MM metadynamics simulations were performed to investigate the conformational preferences of 4NPMan or 4NPGlc bound to the Os7BGlu26 active site. Using the Cremer−Pople θ and ϕ puckering coordinates as collective variables, the free energies of all conformations of the D-mannosyl and D-glucosyl moieties were calculated and mapped as a Mercator projection in Figure 4. The FEL of the D-glucosyl

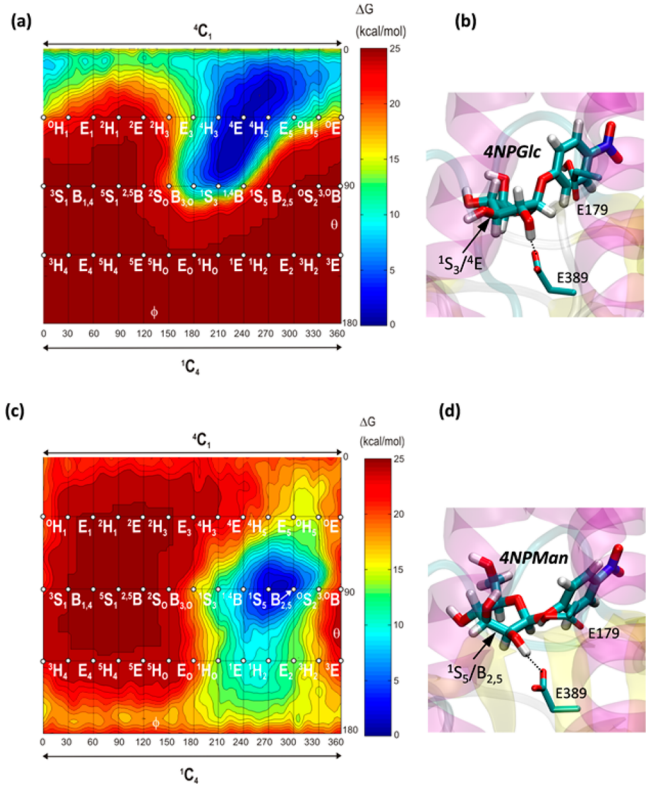

Figure 4. (a, c) Conformational free energy landscapes of (a) the D-glucosyl moiety of 4NPGlc bound to the Os7BGlu26 active site and (c) the D-mannosyl moiety of 4NPMan in the Os7BGlu26 active site, obtained by QM/MM metadynamics simulations. Contour lines are separated by 1 kcal/mol. (b, d) Structures of the active site of Os7BGlu26 with (b) 4NPGlc in its most stable $^1S_3/^4E$ conformation and (d) 4NPMan in its most stable $^1S_5/B_{2,5}$ conformation.

moiety shows a global minimum centered between $^1S_3$ and ^4E, within a long and nearly vertical profile that extends toward the $^4C_1$ pole (Figure 4a). Therefore, Os7BGlu26 restricts the conformational motion of the D-glucosyl group such that conformations along the itinerary $^1S_3/^4E \rightarrow {}^4E^{\ddagger} \rightarrow {}^4C_1$ are energetically

DOI: 10.1021/acscatal.5b01547
ACS Catal. 2015, 5, 6041−6051

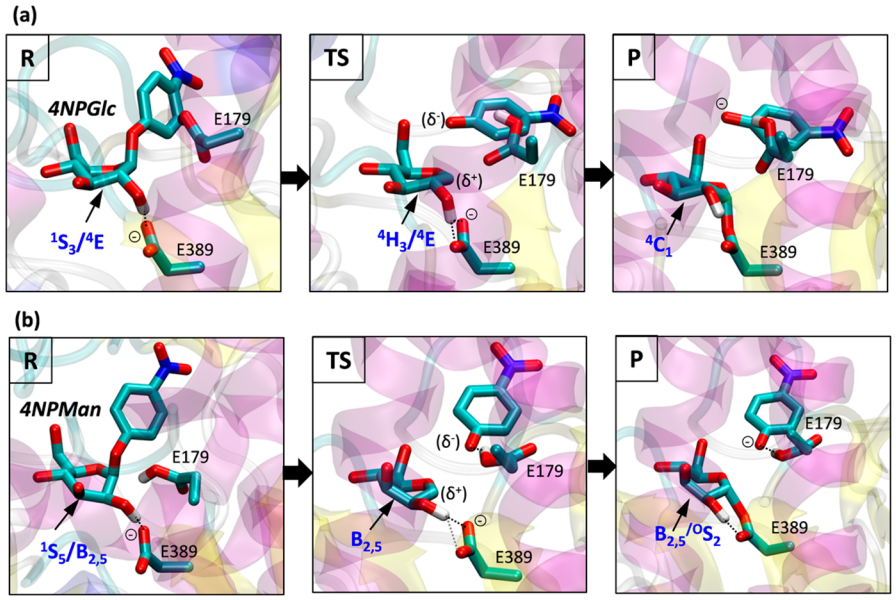

Figure 5. Michaelis complex, transition state, and glycosyl-enzyme intermediate of the glycosylation reaction of (a) 4NPGlc and (b) 4NPMan in the active site of Os7BGlu26 obtained from ab initio QM/MM metadynamics simulations. Both TS forms are very dissociative; thus, no partial bonds to the leaving group and nucleophile residue are shown at the TS.

preferred. This is further supported by QM/MM metadynamics simulations of the glycosyl transfer reaction (Figure 5a and Figure S3 in the Supporting Information), in which the glucose ring evolves from a $^1S_3/^4E$ conformation to an oxocarbenium ion like transition state featuring a mixture of $^4H_3$ and ^4E conformations.

Similar calculations performed on 4NPMan give strikingly different results in comparison to 4NPGlc. The FEL of the D-mannosyl moiety shows a global minimum located in a different region of the Mercator diagram, between $^1S_5$ and $B_{2,5}$ (Figure 4b). As noted for the crystal structures and by others,[74] for superimposed D-mannose $^1S_5/B_{2,5}$ and D-glucose $^1S_3/^4E$ conformations, the O2 atoms lie in essentially the same place in space. The $^1S_5/B_{2,5}$ conformation of the D-mannosyl group is particularly favored in terms of energy, as it enables the 2-OH group to interact strongly with one of the carboxylate oxygen atoms of the nucleophile (an interaction similar to that of the D-glucosyl group in a $^1S_3$ conformation), which would not be possible for the D-mannosyl group in any of the conformations of a $^1S_3 \rightarrow {}^4E^{\ddagger} \rightarrow {}^4C_1$ itinerary. The conformational itinerary of the reaction of the β-D-mannoside substrate was also explored by QM/MM metadynamics simulations of the glycosylation reaction, and an oxocarbenium ion like transition state with a $B_{2,5}$ conformation was observed (Figure 5b).

Assessing Transition State Mimicry of Glucoimidazole. Mannoimidazole, glucoimidazole, and isofagomine are sugar-shaped heterocyclic inhibitors of glycosidases. A design rationale underpinning the use of these molecules is to mimic aspects of the structural and electronic properties of the TS of the hydrolysis reaction:[7,24] namely, the positive charge at the anomeric carbon, the planarity of the C5−O5−C1−C2 atom system, and the orientation of the lone pair of electrons on the "anomeric" nitrogen (in the case of the glycoimidazoles) (see Figure 1). Nevertheless, the degree of transition state mimicry of these inhibitors differs. For mannoimidazole, the mechanistically relevant boat ($^{2,5}B$ and $B_{2,5}$), half-chair ($^4H_3$ and $^3H_4$), and envelope (^3E, E_3, ^4E, and E_4) conformations (hereafter referred to as TS-like conformations) appear in accessible regions in its conformational FEL. In contrast, isofagomine is a poor mimic of TS conformation, as its FEL is strongly biased toward the $^4C_1$ and $^1C_4$ chair conformations;[39] indeed, in the complex reported here, isofagomine binds in a non-TS-like $^4C_1$ conformation, suggesting that the intrinsic conformational preferences of the inhibitor overwhelm those of the enzyme. To date, the FEL for glucoimidazole has not been reported, and thus the relationship between the energetically preferred conformations and those seen on enzyme is not known. We therefore computed the conformational FEL of glucoimidazole, following the same procedure used for mannoimidazole.[39] Figure 6 reveals that the FEL of glucoimidazole is qualitatively similar to that of mannoimidazole, with the TS-like conformations appearing in accessible regions, and with $^4H_3$ and $^3H_4$ conformations representing local minima. Therefore, these two glycoimidazoles should be able to adopt any of the TS-like conformations with only small energetic costs, with the inference that the conformations observed are those induced by specific interactions of the inhibitors with the enzyme active site. Since the free energy of TS binding is thought to be proportional to the logarithm of k_{cat}/K_M of the substrate,[75] and given that Os7BGlu26 possess a clear preference for mannoside hydrolysis with both fast and slow substrates of 1−2 kcal/mol (calculated using $\Delta G = -RT \ln (k_{cat}/K_M)$), it may be expected that a mannoside TS mimic should bind more tightly than a glucoside TS mimic. However, the inhibition data in Table 2 shows the opposite preference by 5 kcal/mol. Careful consideration of the FELs of the imidazoles provides a partial rationale for why glucoimidazole binds more tightly than mannoimidazole to all three enzymes. The K_i value observed for each inhibitor can be considered as the product of the intrinsic affinity of the conformationally matched inhibitor for the enzyme, and the probability that the conformation is present in solution. The FELs reveal that while a $B_{2,5}$ conformation of mannoimidazole is energetically accessible, it lies some 6 kcal mol^{-1} higher in energy than the ground state E_3 conformation and thus is a relatively rare conformation. On the other hand, the ^4E conformation of glucoimidazole lies only 3 kcal mol^{-1} higher in energy than the ground state $^3H_4$

DOI: 10.1021/acscatal.5b01547
ACS Catal. 2015, 5, 6041−6051

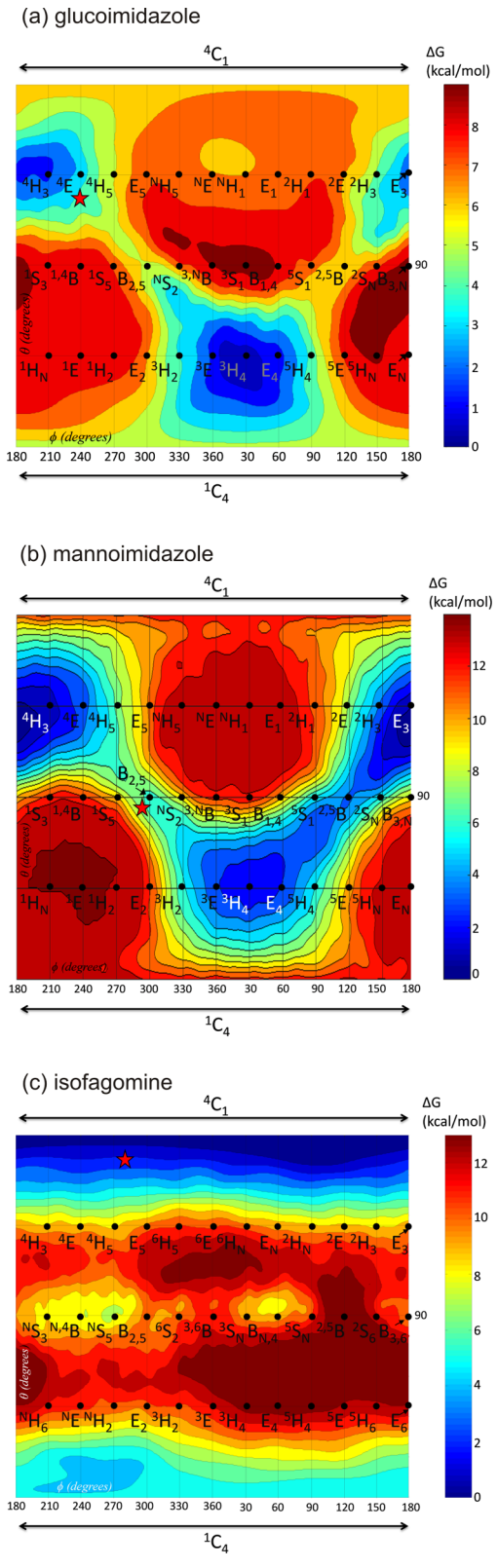

Figure 6. Comparison of the in vacuo free energy landscapes (FELs) of (a) glucoimidazole (this work), (b) mannoimidazole,[39] and (c) isofagomine.[39] The conformations of the inhibitors observed in the crystal structures reported here are indicated by red stars in the corresponding FEL. Contour lines are separated by 1 kcal/mol. Half-chair and envelope conformers are approximately displayed at θ = 45, 135°.

conformations and thus is significantly more populated in solution.[76] The FELs therefore predict an intrinsically tighter binding (in terms of K_i values) of glucoimidazole for all three enzymes studied here, in spite of the kinetic preferences of Os7BGlu26 and HvBII (in terms of k_{cat}/K_M) for D-mannoside substrates.

According to the above analysis, the differences in the energy required to achieve the conformationally matched TS conformation of the inhibitor calculated from the FELs explain only about half of the variation between the energy of TS stabilization for D-glucoside and D-mannoside substrates and that of inhibitor binding for glucoimidazole and mannoimidazole. One approach to assessing transition state mimicry, as espoused by Bartlett, is to plot the change in transition state binding (as log (K_M/k_{cat})) versus the change in inhibitor binding (log K_i) for equivalent modifications to substrate and inhibitor.[75] For a perfect TS mimic a line of slope 1 should result. This form of linear free energy analysis assumes that variations in substrate and inhibitor structure will result in small perturbations and yield a qualitatively similar TS. However, the work presented here shows that the enzymatic reaction coordinates for the two epimeric substrates proceed via fundamentally different TS structures and are unsuited to Bartlett analysis. Thus, while we ascribe around half of the energetic differences in catalytic proficiency versus inhibitor binding to differences in the energy required to adopt a transition state mimicking conformation for D-*gluco*- versus D-*manno*-configured inhibitors, we ascribe the remaining energy deficit to differences in the imperfect mimicry of the inhibitors for the distinct geometric and electronic characteristics of the TSs for β-D-glucoside and β-D-mannoside hydrolysis.

CONCLUSIONS

Previous work has shown that identically configured substrates are hydrolyzed through different conformational itineraries on different glycosidases.[20] For example, β-xyloside hydrolysis by retaining β-xylanases proceeds via a $^1S_3 \rightarrow {}^4H_3{}^{\ddagger} \rightarrow {}^4C_1$ itinerary for GH10 and a $^2S_O \rightarrow {}^{2,5}B^{\ddagger} \rightarrow {}^5S_1$ itinerary for GH11;[69,77] α-mannoside hydrolysis by α-mannosidases can proceed via a $^OS_2 \rightarrow B_{2,5}{}^{\ddagger} \rightarrow {}^1S_5$ itinerary for the retaining families GH38, GH76, and GH92 and a $^3S_1 \rightarrow {}^3H_4{}^{\ddagger} \rightarrow {}^1C_4$ itinerary for the inverting family GH47.[20,78] Similarly, different itineraries have been proposed for different enzymes of the same family, including GH26 β-mannanases ($^OS_2 \rightarrow B_{2,5}{}^{\ddagger} \rightarrow {}^1S_5$) versus β-lichenases/1,3-xylanases ($^1S_3 \rightarrow {}^4E^{\ddagger} \rightarrow {}^4C_1$).[79] The present work is significant in defining the conformational itineraries of Os7BGlu26, a *single enzyme* possessing a dual capacity to hydrolyze β-D-glucosides and β-D-mannosides. X-ray structures of Os7BGlu26 in complexes with glucoimidazole and mannoimidazole reveal distinct $^4H_3$ and $B_{2,5}$ conformations characteristic of widely accepted transition state conformations for β-glucosidases and β-mannosidases, respectively. Additionally, QM calculations show that glucoimidazole, like mannoimidazole, can be considered an informative mimic of TS conformation owing to the energetic accessibility of TS-like conformations, whereas isofagomine possesses an inherently strong conformational bias to a mechanistically uninformative $^4C_1$ conformation. FEL analysis reveals that the energy required to distort mannoimidazole from a half-chair ground state conformation to the TS-mimicking $B_{2,5}$ conformation is greater than that required for distortion of glucoimidazole from a ground state half-chair to a TS-mimicking ^4E conformation, thereby partially explaining the poorer inhibitory potency of the former compound.

When they are bound to Os7BGlu26, mannoimidazole and glucoimidazole adopt distinctive $B_{2,5}$ and ^4E conformations, respectively, which match the TS conformations predicted by ab

DOI: 10.1021/acscatal.5b01547
ACS Catal. 2015, 5, 6041−6051

initio QM/MM metadynamics analysis of 4NPMan and 4NPGlc substrates bound to enzyme. The distinct TS conformations were further assessed by QM/MM metadynamics simulations of the glycosylation reaction: whereas 4NPGlc passes through a $^4H_3/^4E$ oxocarbenium ion like TS, the reaction for 4NPMan takes place via a $B_{2,5}$ TS conformation. The two distinct TS conformations arise in part from the conformational coincidence that places the 2-OH group of a D-glucopyranoside in a ^4E conformation in approximately the same place as the 2-OH group of a D-mannopyranoside in a $B_{2,5}$ conformation. This positional similitude has previously been identified to explain how isofagomine lactam can achieve broad spectrum inhibition of distinct β-glucosidases and β-mannosidases[74] but has not previously been proposed within a single dual-acting glycosidase. The present data demonstrate that a similar principle underlies the ability of Os7BGlu26 to act as a dual β-glucosidase/β-mannosidase and are consistent with its ability to harness different conformational itineraries and distinct transition state conformations on the same enzyme: a $^1S_3 \rightarrow {}^4E^{\ddagger} \rightarrow {}^4C_1$ conformational itinerary for 4NPGlc hydrolysis and a $^1S_5 \rightarrow B_{2,5}{}^{\ddagger} \rightarrow {}^OS_2$ itinerary for 4NPMan hydrolysis. The subtle differences in the positioning of active site residues to favor binding to the 3-OH and 2-OH atoms in the $^4E^{\ddagger}$ conformation for Os3BGlu7 or the $B_{2,5}{}^{\ddagger}$ conformation for Os7BGlu26 are most likely the major contributors to the transition state binding preference that determines the specificity for β-D-glucosides versus β-D-mannosides. Whether enzymes with a strong preference for β-D-glucosides use a $^1S_5 \rightarrow B_{2,5}{}^{\ddagger} \rightarrow {}^OS_2$ conformational itinerary for β-D-mannoside hydrolysis or utilize other mechanisms to control substrate specificity warrants further study.

■ ASSOCIATED CONTENT

Supporting Information

The Supporting Information is available free of charge on the ACS Publications website at DOI: 10.1021/acscatal.5b01547.

X-ray crystallographic data collection, processing, and model statistics of Os7BGlu26 complexes with mannoimidazole (MIM), glucoimidazole (GIM), and isofagomine (IFG), slow onset inhibition of Os7BGlu26 with inhibitors consistent with transition state mimicry, superposition of the active site of Os3BGlu7 β-glucosidase in complex with cellotetraose and the Os7BGlu26 β-mannosidase in complex with glucoimidazole or mannoimidazole, emphasizing interactions at OH3, free energy profiles obtained from the QM/MM metadynamics simulations of the glycosylation reaction for the 4NPGlc and 4NPMan complexes, and structures of inhibitors (PDF)

■ AUTHOR INFORMATION

Corresponding Authors

*E-mail for C.R.: c.rovira@ub.edu.
*E-mail for S.J.W.: sjwill@unimelb.edu.au.
*E-mail for J.R.K.C.: cairns@sut.ac.th.

Notes

The authors declare no competing financial interest.

■ ACKNOWLEDGMENTS

We thank Giovanni Bussi and Alejandro Ley for help in implementing the puckering coordinates for six-membered rings as collective variables in Plumed2. This work was supported by the Thailand Research Fund Grant BRG5680012, the Strategic Scholarships for Frontier Research Network Ph.D. Program, the National Research University Project to Suranaree University of Technology from the Commission on Higher Education of Thailand, the Generalitat de Catalunya (2014SGR-987), the Spanish Ministry of Economy and Competitiveness (CTQ2014-55174-P), and the Australian Research Council through a Future Fellowship. R.C.R. thanks A*STAR Singapore for support. S.B. was supported by a Royal Golden Jubilee Ph.D. Scholarship (Grant PHD/106/2551) from the Thailand Research Fund. We acknowledge the computer support, technical expertise, and assistance provided by the Barcelona Supercomputing Center-Centro Nacional de Supercomputación (BSC-CNS). Data collection was carried out at the National Synchrotron Radiation Research Center (NSRRC), a national user facility supported by the National Science Council of Taiwan, ROC. The Synchrotron Radiation Protein Crystallography Facility is supported by the National Research Program for Genomic Medicine.

■ REFERENCES

(1) Ketudat Cairns, J. R.; Esen, A. *Cell. Mol. Life Sci.* **2010**, *67*, 3389−3405.
(2) Spiro, R. G. *Cell. Mol. Life Sci.* **2004**, *61*, 1025−1041.
(3) Lombard, V.; Golaconda Ramulu, H.; Drula, E.; Coutinho, P. M.; Henrissat, B. *Nucleic Acids Res.* **2014**, *42*, D490−D495.
(4) McCleary, B. V.; Matheson, N. K. *Phytochemistry* **1975**, *14*, 1187−1194.
(5) Wang, C. Y.; Chiou, C. Y.; Wang, H. L.; Krishnamurthy, R.; Venkatagiri, S.; Tan, J.; Yeh, K. W. *Planta* **2008**, *227*, 1063−1077.
(6) Chauhan, P. S.; Puri, N.; Sharma, P.; Gupta, N. *Appl. Microbiol. Biotechnol.* **2012**, *93*, 1817−1830.
(7) Vasella, A.; Davies, G. J.; Bohm, M. *Curr. Opin. Chem. Biol.* **2002**, *6*, 619−629.
(8) Davies, G. J.; Mackenzie, L.; Varrot, A.; Dauter, M.; Brzozowski, A. M.; Schulein, M.; Withers, S. G. *Biochemistry* **1998**, *37*, 11707−11713.
(9) Ducros, V. M.; Zechel, D. L.; Murshudov, G. N.; Gilbert, H. J.; Szabo, L.; Stoll, D.; Withers, S. G.; Davies, G. J. *Angew. Chem., Int. Ed.* **2002**, *41*, 2824−2827.
(10) Davies, G. J.; Ducros, V. M.; Varrot, A.; Zechel, D. L. *Biochem. Soc. Trans.* **2003**, *31*, 523−527.
(11) Tailford, L. E.; Offen, W. A.; Smith, N. L.; Dumon, C.; Morland, C.; Gratien, J.; Heck, M. P.; Stick, R. V.; Bleriot, Y.; Vasella, A.; Gilbert, H. J.; Davies, G. J. *Nat. Chem. Biol.* **2008**, *4*, 306−312.
(12) Cantarel, B. L.; Coutinho, P. M.; Rancurel, C.; Bernard, T.; Lombard, V.; Henrissat, B. *Nucleic Acids Res.* **2009**, *37*, D233−D238.
(13) Dias, F. M.; Vincent, F.; Pell, G.; Prates, J. A.; Centeno, M. S.; Tailford, L. E.; Ferreira, L. M.; Fontes, C. M.; Davies, G. J.; Gilbert, H. J. *J. Biol. Chem.* **2004**, *279*, 25517−25526.
(14) Tankrathok, A.; Iglesias-Fernandez, J.; Luang, S.; Robinson, R. C.; Kimura, A.; Rovira, C.; Hrmova, M.; Ketudat Cairns, J. R. *Acta Crystallogr., Sect. D: Biol. Crystallogr.* **2013**, *69*, 2124−2135.
(15) Opassiri, R.; Hua, Y.; Wara-Aswapati, O.; Akiyama, T.; Svasti, J.; Esen, A.; Ketudat Cairns, J. R. *Biochem. J.* **2004**, *379*, 125−131.
(16) Hrmova, M.; Burton, R. A.; Biely, P.; Lahnstein, J.; Fincher, G. B. *Biochem. J.* **2006**, *399*, 77−90.
(17) Kuntothom, T.; Luang, S.; Harvey, A. J.; Fincher, G. B.; Opassiri, R.; Hrmova, M.; Ketudat Cairns, J. R. *Arch. Biochem. Biophys.* **2009**, *491*, 85−95.
(18) Xu, Z.; Escamilla-Trevino, L.; Zeng, L.; Lalgondar, M.; Bevan, D.; Winkel, B.; Mohamed, A.; Cheng, C. L.; Shih, M. C.; Poulton, J.; Esen, A. *Plant Mol. Biol.* **2004**, *55*, 343−367.
(19) Zechel, D. L.; Withers, S. G. *Acc. Chem. Res.* **2000**, *33*, 11−18.
(20) Speciale, G.; Thompson, A. J.; Davies, G. J.; Williams, S. J. *Curr. Opin. Struct. Biol.* **2014**, *28*, 1−13.
(21) Sinnott, M. L. *Chem. Rev.* **1990**, *90*, 1171−1202.
(22) Davies, G. J.; Planas, A.; Rovira, C. *Acc. Chem. Res.* **2012**, *45*, 308−316.

DOI: 10.1021/acscatal.5b01547
ACS Catal. 2015, 5, 6041−6051

(23) Vocadlo, D. J.; Davies, G. J. *Curr. Opin. Chem. Biol.* **2008**, *12*, 539−555.
(24) Gloster, T. M.; Vocadlo, D. J. *Nat. Chem. Biol.* **2012**, *8*, 683−694.
(25) Hine, J. In *Advances in Physical Organic Chemistry*; Gold, V., Bethel, D., Eds.; Academic Press: San Diego, CA, 1978; Vol. *15*, p 1.
(26) Sinnott, M. L. In *Advances in Physical Organic Chemistry*; Bethell, D., Ed.; Academic Press: San Diego, CA, 1988; Vol. *24*, p 113.
(27) Varrot, A.; Schülein, M.; Pipelier, M.; Vasella, A.; Davies, G. J. *J. Am. Chem. Soc.* **1999**, *121*, 2621−2622.
(28) Verdoucq, L.; Moriniere, J.; Bevan, D. R.; Esen, A.; Vasella, A.; Henrissat, B.; Czjzek, M. *J. Biol. Chem.* **2004**, *279*, 31796−31803.
(29) Seshadri, S.; Akiyama, T.; Opassiri, R.; Kuaprasert, B.; Ketudat Cairns, J. *Plant Physiol.* **2009**, *151*, 47−58.
(30) Jeng, W. Y.; Wang, N. C.; Lin, M. H.; Lin, C. T.; Liaw, Y. C.; Chang, W. J.; Liu, C. I.; Liang, P. H.; Wang, A. H. *J. Struct. Biol.* **2011**, *173*, 46−56.
(31) Burmeister, W. P.; Cottaz, S.; Rollin, P.; Vasella, A.; Henrissat, B. *J. Biol. Chem.* **2000**, *275*, 39385−39393.
(32) Zechel, D. L.; Reid, S. P.; Stoll, D.; Nashiru, O.; Warren, R. A.; Withers, S. G. *Biochemistry* **2003**, *42*, 7195−7204.
(33) Gloster, T. M.; Roberts, S.; Perugino, G.; Rossi, M.; Moracci, M.; Panday, N.; Terinek, M.; Vasella, A.; Davies, G. J. *Biochemistry* **2006**, *45*, 11879−11884.
(34) Gloster, T. M.; Meloncelli, P.; Stick, R. V.; Zechel, D.; Vasella, A.; Davies, G. J. *J. Am. Chem. Soc.* **2007**, *129*, 2345−2354.
(35) Chuenchor, W.; Pengthaisong, S.; Robinson, R. C.; Yuvaniyama, J.; Svasti, J.; Ketudat Cairns, J. R. *J. Struct. Biol.* **2011**, *173*, 169−179.
(36) Offen, W. A.; Zechel, D. L.; Withers, S. G.; Gilbert, H. J.; Davies, G. J. *Chem. Commun.* **2009**, *18*, 2484−2486.
(37) Wicki, J.; Williams, S. J.; Withers, S. G. *J. Am. Chem. Soc.* **2007**, *129*, 4530−4531.
(38) Ermert, P.; Vasella, A.; Weber, M.; Rupitz, K.; Withers, S. G. *Carbohydr. Res.* **1993**, *250*, 113−128.
(39) Williams, R. J.; Iglesias-Fernandez, J.; Stepper, J.; Jackson, A.; Thompson, A. J.; Lowe, E. C.; White, J. M.; Gilbert, H. J.; Rovira, C.; Davies, G. J.; Williams, S. J. *Angew. Chem., Int. Ed.* **2014**, *53*, 1087−1091.
(40) Chuenchor, W.; Pengthaisong, S.; Robinson, R. C.; Yuvaniyama, J.; Oonanant, W.; Bevan, D. R.; Esen, A.; Chen, C.-J.; Opassiri, R.; Svasti, J.; Ketudat Cairns, J. R. *J. Mol. Biol.* **2008**, *377*, 1200−1215.
(41) Otwinowski, Z.; Minor, W. *Methods Enzymol.* **1997**, *276*, 307−326.
(42) Murshudov, G. N.; Lebedev, A.; Vagin, A. A.; Wilson, K. S.; Dodson, E. J. *Acta Crystallogr., Sect. D: Biol. Crystallogr.* **1999**, *55*, 247−255.
(43) Winn, M. D.; Ballard, C. C.; Cowtan, K. D.; Dodson, E. J.; Emsley, P.; Evans, P. R.; Keegan, R. M.; Krissinel, E. B.; Leslie, A. G.; McCoy, A.; McNicholas, S. J.; Murshudov, G. N.; Pannu, N. S.; Potterton, E. A.; Powell, H. R.; Read, R. J.; Vagin, A.; Wilson, K. S. *Acta Crystallogr., Sect. D: Biol. Crystallogr.* **2011**, *67*, 235−242.
(44) Emsley, P.; Cowtan, K. *Acta Crystallogr., Sect. D: Biol. Crystallogr.* **2004**, *60*, 2126−2132.
(45) Laskowski, R. A.; MacArthur, M. W.; Moss, D. S.; Thornton, J. M. *J. Appl. Crystallogr.* **1993**, *26*, 283−291.
(46) Chen, V. B.; Arendall, W. B.; Headd, J. J.; Keedy, D. A.; Immormino, R. M.; Kapral, G. P.; Murray, L. W.; Richardson, J. S.; Richardson, D. C. *Acta Crystallogr., Sect. D: Biol. Crystallogr.* **2010**, *66*, 12−21.
(47) Cremer, D.; Pople, J. A. *J. Am. Chem. Soc.* **1975**, *97*, 1354−1358.
(48) Baiya, S.; Hua, Y.; Ekkhara, W.; Ketudat Cairns, J. R. *Plant Sci.* **2014**, *227*, 101−109.
(49) Dixon, M. *Biochem. J.* **1953**, *55*, 170−171.
(50) Mosteller, F.; Turkey, J. W. *Data analysis and regression*; Addison-Wesley: Reading, PA, 1977; p 353.
(51) McIntosh, L. P.; Hand, G.; Johnson, P. E.; Joshi, M. D.; Körner, M.; Plesniak, L. A.; Ziser, L.; Wakarchuk, W. W.; Withers, S. G. *Biochemistry* **1996**, *35*, 9958−9966.
(52) Case, D. A.; Darden, T. A.; Cheatham, T. E.; Simmerling, C.; Wang, J.; Duke, R.; Luo, R.; Crowley, M. F.; Walker, R.; Zhang, W.; Merz, K. M.; Wang, B.; Hayik, S.; Roitberg, A. E.; Seabra, G.; Kolossváry, I.; Wong, K. F.; Paesani, F.; Vanicek, J.; Wu, X.; Brozell, S.; Steinbrecher, T.; Gohlke, H.; Yang, L.; Tan, C.; Mongan, J.; Hornak, V.; Cui, G.; Mathews, D. H.; Seetin, M. G.; Sagui, C.; Babin, V.; Kollman, P. *Amber 11*; University of California: San Francisco, CA, 2010; p 1.
(53) Hornak, V.; Abel, R.; Strockbine, B.; Roitberg, A.; Simmerling, C. *Proteins: Struct., Funct., Genet.* **2006**, *65*, 712−725.
(54) Kirschner, K. N.; Yongye, A. B.; Tschampel, S. M.; Gonzalez-Outeirino, J.; Daniels, C. R.; Foley, B. L.; Woods, R. J. *J. Comput. Chem.* **2008**, *29*, 622−655.
(55) Frisch, M. J.; Trucks, G. W.; Schlegel, H. B.; Scuseria, G. E.; Robb, M. A.; Cheeseman, J. R. *GAUSSIAN 03*; Gaussian Inc., Wallingford, CT, 2004.
(56) Jorgensen, W. L.; Chandrasekhar, J.; Madura, J. D.; Impey, R. W.; Klein, M. L. *J. Chem. Phys.* **1983**, *79*, 926−935.
(57) Essmann, U.; Perera, L.; Berkowitz, M. L.; Darden, T.; Lee, H.; Pedersen, L. G. *J. Chem. Phys.* **1995**, *103*, 8577−8593.
(58) Berendsen, H. J. C.; Postma, J. P. M.; van Gunseteren, W. F.; Dinola, A.; Haak, J. R. *J. Chem. Phys.* **1984**, *81*, 3684−3690.
(59) Humphrey, W.; Dalke, A.; Schulten, K. *J. Mol. Graphics* **1996**, *14*, 33−38.
(60) Laio, A.; Van de Vondele, J.; Rothlisberger, U. *J. Chem. Phys.* **2002**, *116*, 6941−6947.
(61) Car, R.; Parrinello, M. *Phys. Rev. Lett.* **1985**, *55*, 2471−2474.
(62) Troullier, N.; Martins, J. L. *Phys. Rev. B: Condens. Matter Mater. Phys.* **1991**, *43*, 1993−2006.
(63) Perdew, J. P.; Burke, K.; Ernzerhof, M. *Phys. Rev. Lett.* **1996**, *77*, 3865−3868.
(64) Biarnés, X.; Ardèvol, A.; Planas, A.; Rovira, C.; Laio, A.; Parrinello, M. *J. Am. Chem. Soc.* **2007**, *129*, 10686−10693.
(65) Ardèvol, A.; Biarnés, X.; Planas, A.; Rovira, C. *J. Am. Chem. Soc.* **2010**, *132*, 16058−16065.
(66) Lammerts van Bueren, A.; Ardèvol, A.; Fayers-Kerr, J.; Luo, B.; Zhang, Y.; Sollogoub, M.; Blériot, Y.; Rovira, C.; Davies, G. J. *J. Am. Chem. Soc.* **2010**, *132*, 1804−1806.
(67) Thompson, A. J.; Dabin, J.; Iglesias-Fernandez, J.; Ardèvol, A.; Dinev, Z.; Williams, S. J.; Bande, O.; Siriwardena, A.; Moreland, C.; Hu, T. C.; Smith, D. K.; Gilbert, H. J.; Rovira, C.; Davies, G. J. *Angew. Chem., Int. Ed.* **2012**, *51*, 10997−11001.
(68) Passos, O.; Fernandes, P. A.; Ramos, M. J. *Theor. Chem. Acc.* **2011**, *129*, 119−129.
(69) Iglesias-Fernández, J.; Raich, L.; Ardèvol, A.; Rovira, C. *Chem. Sci.* **2015**, *6*, 1167−1177.
(70) Barducci, A.; Bussi, G.; Parrinello, M. *Phys. Rev. Lett.* **2008**, *100*, 20603−20604.
(71) Tribello, G. A.; Bonomi, M.; Branduardi, D.; Camilloni, C.; Bussi, G. *Comput. Phys. Commun.* **2014**, *185*, 604−613.
(72) Lohse, A.; Hardlei, T.; Jensen, A.; Plesner, I. W.; Bols, M. *Biochem. J.* **2000**, *349*, 211−215.
(73) Panday, N.; Canac, Y.; Vasella, A. *Helv. Chim. Acta* **2000**, *83*, 58−79.
(74) Vincent, F.; Gloster, T. M.; Macdonald, J.; Morland, C.; Stick, R. V.; Dias, F. M.; Prates, J. A.; Fontes, C. M.; Gilbert, H. J.; Davies, G. J. *ChemBioChem* **2004**, *5*, 1596−1599.
(75) Mader, M. M.; Bartlett, P. A. *Chem. Rev.* **1997**, *97*, 1281−1301.
(76) Force-field-based studies have shown that the water environment does not significantly affect the conformational FEL of *β*-glucose: Spiwok, V.; Králová, B.; Tvaroska, I. *Carbohydr. Res.* **2010**, *345*, 530−537. Therefore, the FELs computed here for the isolated molecules can be taken as an approximation of the solution FELs.
(77) Notenboom, V.; Williams, S. J.; Hoos, R.; Withers, S. G.; Rose, D. R. *Biochemistry* **2000**, *39*, 11553−11563.
(78) Thompson, A. J.; Speciale, G.; Iglesias-Fernández, J.; Hakki, Z.; Belz, T.; Cartmell, A.; Spears, R. J.; Chandler, E.; Temple, M. J.; Stepper, J.; Gilbert, H. J.; Rovira, C.; Williams, S. J.; Davies, G. J. *Angew. Chem., Int. Ed.* **2015**, *54*, 5378−5382.
(79) Money, V. A.; Smith, N. L.; Scaffidi, A.; Stick, R. V.; Gilbert, H. J.; Davies, G. J. *Angew. Chem., Int. Ed.* **2006**, *45*, 5136−5140.
(80) Fersht, A. *Structure and Mechanism in Protein Science*; W. H. Freeman: New York, 1999; p 1.

DOI: 10.1021/acscatal.5b01547
ACS Catal. 2015, 5, 6041−6051